Journal of Molecular Catalysis A: Chemical 335 (2011) 112–120

Contents lists available at ScienceDirect

Journal of Molecular Catalysis A: Chemical

journal homepage: www.elsevier.com/locate/molcata

Interpretation of the catalytic functionalities of CoMo/ASA FCC-naphtha-HDT catalysts based on its acid properties

David J. Pérez-Martínez[a], Eric M. Gaigneaux[b], Sonia A. Giraldo[a], Aristóbulo Centeno[a,*]

[a] Centro de Investigaciones en Catálisis (CICAT), Escuela de Ingeniería Química, Universidad Industrial de Santander (UIS), Cra 27, Calle 9, Bucaramanga, Colombia
[b] Université Catholique de Louvain, Institute of Condensed Matter and Nanoscience (IMCN)[1], Division Molecules Solids and Reactivity (MOST)[1], Croix du Sud 2/17, 1348 Louvain-La-Neuve, Belgium

ARTICLE INFO

Article history:
Received 2 August 2010
Received in revised form 8 November 2010
Accepted 20 November 2010
Available online 26 November 2010

Keywords:
CoMo
FCC naphtha HDT
Amorphous aluminosilicates
HDS
Brönsted/Lewis ratio

ABSTRACT

CoMo catalysts supported on amorphous aluminosilicates (ASA) with different Si/(Si + Al) ratios (0, 0.15, 0.25, 0.33, 0.5, and 0.75) were prepared and evaluated in the hydrotreatment of synthetic FCC naphtha. 2-Methylthiophene was used as the sulfur compound, and a mixture of 2,4,4-trimethyl-1-pentene and 2,4,4-trimethyl-2-pentene (approximately 3:1) was used as olefin. With the increase of Si/(Si + Al) ratio, the activity of hydrodesulfurization (HDS) and hydrogenation of olefin (HYDO) reactions performed in the CUS sites of Mo promoted by Co was inhibited. Meanwhile, increments in the acid-type reactions (alkylation of 2-MT with olefins and olefin isomerization and cracking) were observed. These changes were not gradual; a kind of transition zone with huge changes in product distribution between catalysts with 15 and 25% Si/(Si + Al) was observed. This was explained by an increment in the density and strength of Brönsted sites. These Brönsted sites compete with the CUS sites of Mo promoted by Co for reactant adsorption. Moreover, it was shown that skeletal isomerization could aid to control HYDO and cracking reactions. In general, it was demonstrated that by modifying the support composition, it is possible to modify the hydrodesulfurization, hydrogenation of olefins, and acid-type reaction activities.

1. Introduction

It is well known that olefins present in the FCC naphtha are a major contribution to the octane number in gasoline [1–3]. Thus, it is imperative to eliminate the maximum amount of sulfur impurities impeding olefin saturation during the hydrotreatment (HDT) of FCC naphtha [1–3]. Despite the process, it has been shown that catalyst selectivity is the key to achieve this goal [4–7]. In the case of selective classical HDS, various attempts to develop selective catalysts for this purpose are found in literature [1–5,8–13]. Support modification appears to be a good approach to obtaining more selective catalysts. In this sense, the investigations have been focused on the use of supports less acidic than alumina [1,8,9]. Some improvements in the hydrodesulfurization/hydrogenation of olefin (HDS/HYDO) selectivity have been encountered using this kind of supports; however, a loss of activity was also found in comparison to the conventional CoMo/γ-Al_2O_3. On the other hand, although some references about improvements in the HDS/HYDO selectivity using more acidic catalysts can be found [10,11], a detailed explanation of this behavior based on its acid properties and its influence in the catalytic performance was not given. Consequently, there is still a lack of information about not only the catalytic performance of CoMo catalysts supported on acid-type materials in the HDT of FCC naphtha, but also the influence of changes of the different acid properties. Thus, the particular influence of the acid–base properties of catalysts on the selectivity to HDS in the HDT of FCC naphtha is not yet clear.

In this work, the performance of amorphous-aluminosilicate-supported CoMo catalysts with different Si/(Si + Al) ratios in the HDT of a synthetic FCC naphtha was studied in order to determine the influence of support composition on the catalyst acid properties and the influence of these acid properties on the catalytic functions: HDS, HYDO, and acidity.

2. Experimental

2.1. Preparation of catalysts

Amorphous aluminosilicate (ASA) supports with different Si/(Si + Al) ratios (0.15, 0.25, 0.33, 0.5 and 0.75) were prepared by the sol–gel route following a procedure similar to the one described by La Parola et al. [14] using aluminum tri-sec-butoxide (Aldrich, 97%) and tetraethyl orthosilicate (Aldrich, 98%) as precursors. In

* Corresponding author. Tel.: +57 7 6344746; fax: +57 7 6344684.
E-mail addresses: acenteno@uis.edu.co, davidjpmtz@hotmail.com (A. Centeno).

[1] IMCN and MOST are new research entities emerging from the reorganization of the Université catholique de Louvain, and integrating the laboratory formerly known as Unité de catalyse et chimie des matériaux divisés.

1381-1169/$ – see front matter © 2010 Elsevier B.V. All rights reserved.
doi:10.1016/j.molcata.2010.11.022

order to check the reproducibility of the preparation method, the syntheses of supports with the same Al/Si ratios were repeated at least twice. CoMo catalysts supported on ASA containing 10% MoO_3 and 2% CoO were prepared by successive incipient wetness impregnation. The supports and the catalysts were named ASAxx and CMSxx, respectively, where xx represents the % of Si/(Si + Al). An initial impregnation step was performed with an aqueous solution of $(NH_4)_6Mo_7O_{24}{\cdot}4H_2O$ (Merck), subsequently the solids were impregnated with an aqueous solution of $Co(NO_3)_2{\cdot}6H_2O$. After each impregnation step, solids were dried under airflow at 343 K for 2 h and air calcined at 773 K for 12 h. A conventional CoMo catalyst supported on a commercial γ-Al_2O_3 (Procatalyse), named here CMA, was also prepared by the same method for comparison purposes. In this case, after each impregnation step, the solids were dried under airflow at 393 K for 12 h and, finally, air calcined at 773 K for 4 h. Additionally, CoMo catalysts supported on mechanical mixtures of silica and alumina with the same Si/(Si + Al) ratios of the ASAxx supports were also prepared for comparison purposes.

2.2. Characterization of catalysts

2.2.1. Catalysts composition

The catalyst and support nominal compositions were verified by X-ray fluorescence (XRF) using a Shimadzu EDX 800 HS apparatus.

2.2.2. Textural properties

The specific surface area (A_{BET}) of both catalysts and supports was estimated by the BET method using N_2 adsorption–desorption isotherms obtained with a Quantachrome NOVA 1200 instrument. The solids were previously outgassed in vacuum (1×10^{-3}) all night at 70 °C.

2.2.3. Acid properties

Acid properties of both catalysts and supports in the oxide state were determined by NH_3 temperature programmed desorption (TPD) and Fourier transformed infrared (FT-IR) spectra of adsorbed pyridine.

For NH_3 TPD experiments, outlet gases were analyzed with a mass spectrometer equipped with a quadrupole mass filter (Balzers QMC 200). The samples (100 mg) were first dehydrated under pure He at 773 K until obtaining a flat-water signal (m/z 17 and 18). Then, samples were cooled down under He flow to room temperature (RT). NH_3 adsorption was then performed by passing across the samples a flow of 5% NH_3 in He. Excess NH_3 was evacuated at RT by passing a flow of pure He until obtaining a flat NH_3 signal (m/z 15, 16 and 17). Desorption of the adsorbed NH_3 was performed by increasing temperature from RT to 873 K at 10 K min^{-1}. The signal corresponding to m/z of 16, assigned to NH_3, was used for the analysis of the NH_3 TPD curves.

FT-IR spectra of pre-adsorbed pyridine were recorded with an IFS55 equinox spectrometer (Brücker) equipped with a DTGS detector, using 100 scans and a resolution of 4 cm^{-1}. Catalyst and support powders were pressed (3 tons) into self-supported wafers (15 mg, 13 mm diameter) and placed in a homemade IR cell. Samples were first dehydrated under vacuum (<1×10^{-5} mbar) at 773 K for 2 h. After cooling down to RT, a first spectrum was taken as reference. Samples were then exposed to 10 mbar of pyridine for 30 min. FT-IR spectra were recorded after outgassing the samples (<10^{-5} mbar) in four steps of 1 h each: RT, 373, 473 and 573 K.

2.2.4. Confocal laser Raman microscopy (Raman)

Raman was performed with a Labram spectrometer (Dilor) interfaced with an Olympus optical microscope. The excitation radiation was a He–Ne laser (780 nm) operated at a power of 10 mW. The 100× objective of the microscope was used, so that a spot of about 1 μm at the surface of the sample was measured at once. Spectra were obtained by averaging 25 scans of the Raman shift range between 1400 and 100 cm^{-1} recorded in 25 s with a spectral resolution of 1 cm^{-1}. The identity of the spectra obtained at different positions of each sample was verified systematically.

2.2.5. UV–vis diffusive reflectance

UV–vis diffusive reflectance spectra (DRS) of the oxide catalysts were recorded on a UV-2401PC Shimadzu spectrophotometer with an ISR 240A integrating sphere accessory. UV–vis DRS were recorded between 200 and 800 nm using $BaSO_4$ powder as a reference. The Kubelka–Munk function was calculated from reflectance results and plotted against the wavelength.

2.3. Catalytic evaluation

Catalytic tests were made in a continuous-flow stainless-steel fixed-bed reactor. The composition of the model charge was 2 wt.% of 2-methylthiophene (2-MT) and 20 wt.% of olefins dissolved in n-heptane. The olefins used were a commercial mixture of 2,4,4-trimethyl-1-pentene (TM1P) and 2,4,4-trimethyl-2-pentene (TM2P), which are representative of terminal and internal ramified olefins in FCC naphtha (3:1 approximately). Dodecane (2 wt.%) was used as an internal standard for the chromatographic analysis of condensable products. Before reaction, 0.35 g of catalyst (0.18–0.6 mm particle size) was dried in situ under N_2 flow (100 ml min^{-1}) at 393 K for 1 h and subsequently, it was activated with a H_2S/H_2 (15/85, v/v) mixture at 673 K (10 K min^{-1}) for 3 h. Thereafter, the reaction conditions were fixed: 17 MPa, 523 K, liquid-flow rate of 20 ml h^{-1} and H_2/liquid-feed ratio of 500. Under these conditions, the absence of any diffusion limitations was previously verified. Catalytic tests were conducted until reaching the steady state (approximately 6 h). It was considered that the steady state was reached by the reaction system when three consecutive samples of the condensable products, taken each hour, did not present any appreciable changes in their composition. These condensable products were analyzed offline in a HP 6890 gas chromatograph equipped with a HP-1 column (100 m × 0.25 mm × 0.5 μm) and a FID detector. Product identification was performed by GC–MS analyses and by comparing the retention times of some reagent-grade compounds in the FID and FPD detectors in the same column.

2.4. Expression of results

In the case of reactants, the activity was expressed in terms of apparent kinetic constants (k_i) assuming first order rate equations for the total conversion of 2-MT and olefins. After integration of the design equation for a fixed-bed reactor, the following expression of the apparent kinetic constant could be written:

$$k_i = -\frac{F_0}{C_0 \times m}\,\mathrm{Ln}(1 - X) \tag{1}$$

where F_0 is the reactant molar flow in mol h^{-1}, C_0 is the reactant concentration in mol L^{-1}, m the catalyst weight used in g, and X the total conversion. In the case of products, the following equation was used to calculate the yield of product P (Y.P), taking into account the moles of reactant R converted:

$$\mathrm{Y.P} = \frac{\mathrm{mol}\,P_{\mathrm{output}}}{\alpha_{RP} \times (\mathrm{mol}\,R_{\mathrm{input}} - \mathrm{mol}\,R_{\mathrm{output}})} \times 100 \tag{2}$$

α_{RP} is the ratio between the stoichiometric coefficients of product P and reactant R. Selectivity definitions are given inside the text for clarity.

Table 1
Textural properties of ASA supports and CoMo catalysts supported on these.

Si/(Si + Al) ratio	Support	A_{BET} ($m^2\ g^{-1}$)	Catalysts	A_{BET} ($m^2\ g^{-1}$)
0	γ-Al_2O_3	210	CMA	194
15	ASA(15)	397	CMS15	269
25	ASA(25)	550	CMS25	259
33	ASA(33)	378	CMS33	146
50	ASA(50)	508	CMS50	264
75	ASA(75)	117	CMS75	69

3. Results and discussion

3.1. Influence of the Si/(Si + Al) ratio on the catalyst surface properties

Table 1 shows the A_{BET} of catalysts and supports measured by N_2 adsorption–desorption isotherms. From the analysis of the adsorption–desorption curves hysteresis, it can be inferred that all materials are mainly mesoporous with only a small proportion of micropores as expected due to the basic hydrolysis used in the sol–gel synthesis of these materials [14,15]. With the exception of ASA75, all ASA supports presented values of A_{BET} higher than the one of γ-Al_2O_3. Blocking of both the micropores and the smallest mesopores by the active metal deposition could explain the important reduction in the A_{BET} of the CMSxx catalysts, when comparing them with their respective supports [16]. The deterioration of the ASAxx textural properties after active metal incorporation, especially the A_{BET}, has also been reported by other authors [13,14,16].

Fig. 1 presents the total acidity and the acidity strength distribution measured by NH_3 TPD as a function of the Si/(Si + Al) ratio. The zero value in the *X*-axis represents the conventional catalyst CoMo/γ-Al_2O_3. The strength of the acid sites was arbitrarily classified as weak (<423 K), intermediate (423–573 K), and strong (>573) according to the temperature of NH_3 desorption [17]. The values reported represent the percentage of NH_3 desorbed between the temperatures listed above relative to the total NH_3 desorbed. There are almost no substantial changes in the acidity strength distribution with the increase of the Si/(Si + Al) ratio. The only exception was the CMS15 catalyst, where an augmentation in the intermediate acid sites at expense of the weak ones is observed. Total acidity increases with the Si/(Si + Al) ratio and exhibits a maximum around 50% Si/(Si + Al). Similar results were reported by other authors using a similar series of ASA prepared by a different method [18,19].

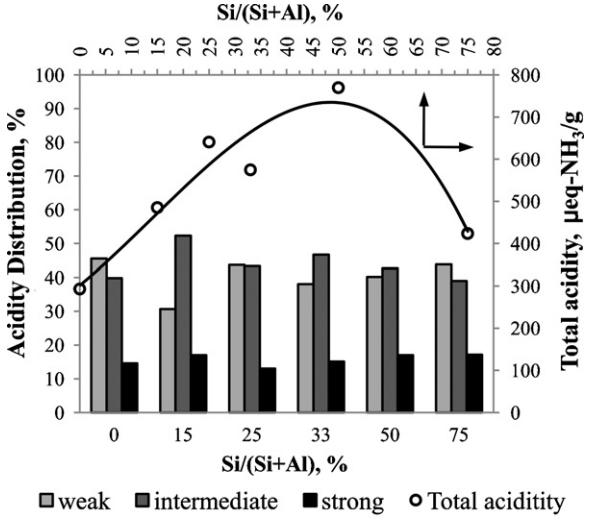

Fig. 1. Total acidity and acidity strength distribution measured by NH_3 TPD of the CoMo catalysts supported on ASA. Weak (T < 423 K), intermediate (423 K < T < 573 K), strong (T > 573).

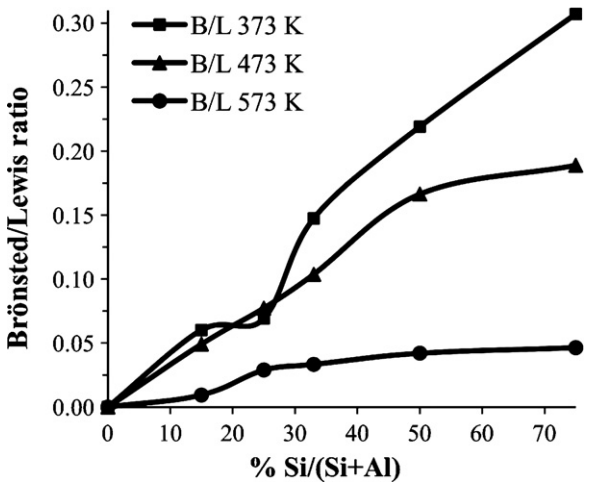

Fig. 2. Brönsted/Lewis ratio of the ASA supported CoMo catalysts determined by FT-IR spectra of adsorbed pyridine after evacuation at 373, 473 and 573 K.

Peaks at 1453 and 1545 cm^{-1} in the IR spectra of adsorbed pyridine (not shown), attributed in literature [14,20] to pyridine bonded to Lewis and Brönsted sites, respectively, were mathematically decomposed using Gauss-type curves. The values resulting from their integration were used to calculate the Brönsted/Lewis ratio, which was plotted as a function of the % of Si/(Si + Al) in Fig. 2. For the CMA catalyst, the Brönsted/Lewis ratio is zero because no Brönsted sites were detected using pyridine as the model molecule, but the Brönsted/Lewis ratio increases continuously when increasing the Si/(Si + Al) ratio. It is also observed that the Brönsted/Lewis ratio decreased after the evacuation at high temperatures, which indicates that there is, comparatively, a higher population of intermediate and strong Lewis acid sites than Brönsted sites.

The increase of the total acidity observed in the CMSxx catalysts in comparison with the one of CMA has been attributed to the formation of a Si–Al mixed phase in the ASA supports [13,14,21]. The substitution of Al in the Si framework or vice versa gives rise to new superficial defects, which create new Lewis and, specially, new Brönsted acid sites [13]. Thus, an indirect way to detect the existence of this Si–Al mixed phase could be the comparison of the activity results in acid-type reactions (cracking and isomerization) of the ASA supported catalysts with the one of catalysts supported on mechanical mixtures of silica and alumina with the same Si/(Si + Al) ratio. These results are showed in Table 2 as the ratio of the activity in the acid-type reaction value of the respective catalyst to the one of the catalyst supported on alumina. It is observed that the activity in acid type reactions of the catalysts supported on mechanical mixtures was similar or even lower than the one of the catalyst supported on alumina. Meanwhile, the one

Table 2
Relative activity in acid-type reactions of CMSxx compared with the one of those supported on silica–alumina mechanical mixtures.

% Si/(Si + Al)	CoMo supported on ASAxx[a]	CoMo supported on silica–alumina mechanical mixtures[a]
0	1.0	1.0
15	2.3	1.1
25	8.1	1.1
33	6.2	1.2
50	8.8	0.5
75	6.4	NA

[a] Results are expressed as the ratio of the activity of the respective catalysts to that of the CMA.

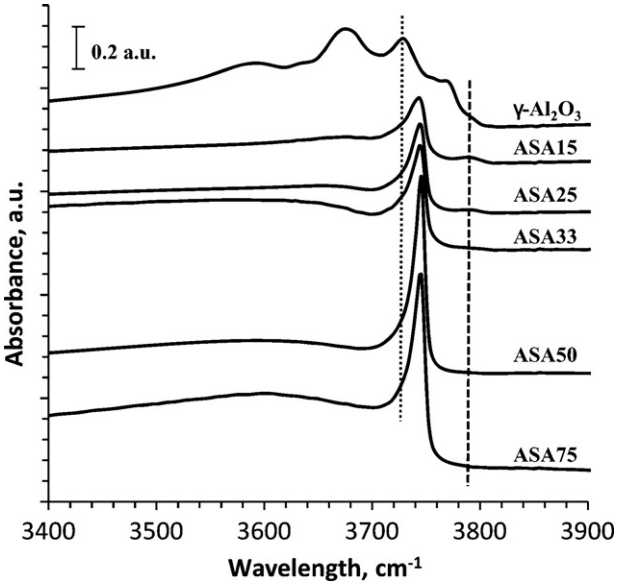

Fig. 3. OH region FT-IR spectra of ASAxx supports compared with pure alumina.

of the catalysts supported on ASA was far higher than the one of the catalyst supported on alumina. This fact suggest the formation of new acid sites in the ASA supports belong to neither silica nor alumina phase; thus, they should be originated during the formation of the Si–Al mixed phase. Additionally, the reduction of the activity in the acid-type reactions of the catalysts supported in the mechanical mixture with 50% Si/(Si + Al) suggests that the only acid sites present on the mechanical mixtures are those belonging to the alumina phase.

The variation of the acid properties of CMSxx catalysts with the Si/(Si + Al) ratio is due to the fact that the Si–Al mixed phase is not formed homogeneously for all the Si/(Si + Al) ratio [21]. In fact, the maximum of the mixed oxide formation has been found between 50 and 75% Si/(Si + Al) [19,21,22], which coincides with the maximum of the total acidity found in Fig. 1 and the maximum of the Brönsted/Lewis ratio found in Fig. 2. According to these authors [19,21,22], below 50% SiO_2 content, the mixed phase is progressively diluted by alumina, which appears as a distinct phase below 40–30% SiO_2 being responsible for the increase in the surface density of Lewis sites as observed in Fig. 2 [21]. As the major part of the catalysts prepared in this work were in that range, the IR spectra of the OH region of dehydrated supports were analyzed in order to identify the existence of different phases in the support surface (Fig. 3). It was found that for ASA supports within the range of 50–75% Si/(Si + Al) ratio, only a peak of silanol groups (at ca. 3750 cm^{-1}) was found [20]. However, in the ASA supports within the range of 15–33% Si/(Si + Al) ratio along with the silanol groups, a little peak ca. 3790 cm^{-1} and a shoulder at ca. 3730 cm^{-1} are also observed. These new bands match well with alumina type IB and IIA OH groups of Knözinger classification [23]. It is observed that these new peaks vanish when increasing the Si/(Si + Al) ratio, even for the CMS33, these are hardly observed. This kind of OH groups was also observed by Bandoz et al. [24] in their protonic acidity distribution (PAD) measurements performed for their silica–alumina supports. Other authors [25] have also observed the existence of Al in octahedral coordination, which is attributable to an alumina distinct phase in the Al^{27} MAS NMR spectra of their ASA.

This heterogeneity of phases present in ASA supports gives rise to some heterogeneity in the nanoscale composition as shown by Sârbu and Delmon [26]. Thus, when the ASA are used as supports for CoMo HDT catalysts, the OH groups that would be available to attach the Mo and Co depend on the Si/(Si + Al) ratio. In consequence, changes in the Mo coordination, speciation and dispersion with variations of the Si/(Si + Al) ratio would be expected. In order to study these changes, the Raman spectra of the catalysts were taken (Fig. 4). First of all, it can be noticed that both Co and Mo are well dispersed on the different supports, because of the lack of peaks characteristic of Co compounds (681, 477 and 199 cm^{-1}) and free MoO_3 aggregates (990–1000 cm^{-1}) [27–29]. Additionally, the presence of $Al_2(MoO_4)_3$ (1000–1010 cm^{-1}) can be ruled out [29]. The CMA catalyst Raman spectrum shows a broad band at ca. 920–950 cm^{-1} with shoulders at both sides ca. 900 and 960 cm^{-1}. There are also other broad bands at ca. 320–360 and 225 cm^{-1}. The region 750–1000 cm^{-1} is where the bands for stretching of Mo–O bonds are typically observed [27,29]. Inside the broad band at ca. 920–950, a variety of Mo species could be placed; the more likely according to literature [27–31] are $Mo_7O_{24}^{6-}$ octahedral species (946–951, 360 and 220 cm^{-1}, continuous lines) and MoO_4^{2-} with distorted tetrahedral symmetry (916 and 320 cm^{-1}, dotted lines). Some contributions from Mo–O–Co stretching vibrations in $CoMoO_4$ species (939, 873, 820, 370 and 340 cm^{-1}, dashed lines) cannot be ruled out [32]. The shoulder at ca. 900 cm^{-1} can be attributed to monomeric undistorted MoO_4^{2-} species (at ca. 892 and 807 cm^{-1}), and the other shoulder at ca. 960 cm^{-1} can be attributed to larger polymeric species such as $Mo_8O_{26}^{4-}$ (958–960 cm^{-1}).

Regarding ASA supported CoMo catalysts in the CMS15 catalyst Raman spectrum, the peaks centered at ca. 915–920 cm^{-1} and at ca. 320 cm^{-1} evidence the majority presence of Mo species with distorted tetrahedral symmetry. Even though a higher frequency shoulder can also be observed around 940–950 cm^{-1}, the presence of $Mo_7O_{24}^{6-}$ octahedral species should be low because no peak close to 225 cm^{-1} is observed. This augmentation in the tetrahedral Mo species when increasing the Si content up to 20 wt.% on ASA was also reported by Vakros et al. [33]. In the CMS25 catalyst spectrum, the shoulder close to 940–950 cm^{-1} is slightly higher in comparison with the one of the CMS15 catalyst, and the peak close to 225 cm^{-1} is now clearly observed. This fact indicates that although the Mo species with distorted tetrahedral symmetry are still majority on the CMS25 catalyst, the population of $Mo_7O_{24}^{6-}$ octahedral species is slightly higher than the one of the CMS15. With the subsequent increments in the Si/(Si + Al) ratio, the population of $Mo_7O_{24}^{6-}$ octahedral species continues increasing at expenses of the population of distorted tetrahedral species.

It is known that the pH of the solution of ammonium heptamolybdate determines the structure of the solution species according to the equilibrium between poly- and monomeric molybdates established in Eqs. (3) and (4) [29]. Thus, at pH values higher than 6.5, the MoO_4^{2-} anion is stable, and a decrease in pH to 4.5 leads to complete formation of $Mo_7O_{24}^{6-}$ [29]. A further decrease in pH to 1.5 leads to polymerization of $Mo_8O_{26}^{4-}$ [29]:

$$Mo_7O_{24}^{6-} + 4H_2O \leftrightarrow 7MoO_4^{2-} + 8H^+ \quad (3)$$

$$Mo_7O_{24}^{6-} + 7MoO_4^{2-} + 2H^+ \leftrightarrow [H_2Mo_8O_{26}]^{6-} \quad (4)$$

Therefore, during the impregnation process, the Mo species, which will be deposited on the support surface, seem to be governed by the surface pH, more precisely, by its point of zero charge (PZC) [29,31]. The surface pH can be drastically altered by chemisorption; therefore, the surface pH is determined by the overall system Mo-oxide/support [29,31]. For instance, alumina has a PZC of 8–9, whereas MoO_3 has a PZC of 1.5. Thus, low Mo loadings (<1 Mo atom/nm^2) on alumina (around 200 $m^2\ g^{-1}$), which are equivalent to high surface pH values, favors the adsorption of MoO_4^{2-} species [29,31]. When increasing the Mo loading, the PZC of the surface drops; therefore, increasing quantities of $Mo_7O_{24}^{6-}$ will be adsorbed. On the other hand, silica has a PZC of 4–5 [13]; thus, using silica as support, pH values high enough for monomolybdate

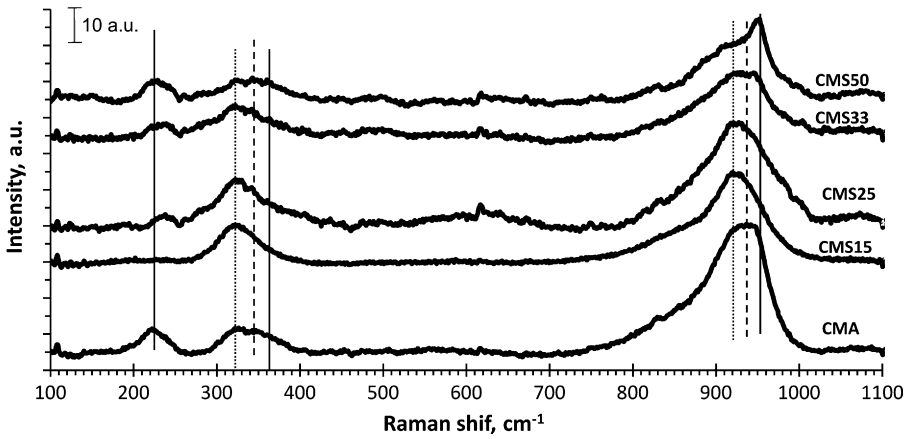

Fig. 4. Raman spectra of the ASAxx supported CoMo catalysts compared with the one supported on alumina. xx: % Si/(Si + Al).

formation are usually not reached. Consequently, under hydrated conditions, only polymeric species will be adsorbed [29]. Also it has been found that Mo is more weakly attached on silica than on alumina leading to the easy formation of MoO_3 [13,27,29].

Therefore, it would be expected that Mo species supported on ASA supports exhibit an intermediate behavior between alumina and silica, i.e., with increasing the Si content the density of polymeric species should increase. However and apparently in contradiction with what has been already said, in Fig. 4 is observed that in the CMS15 catalysts practically only distorted tetrahedral Mo species are present; thus, we have to consider another variable influencing this fact. The 10 wt.% MoO_3 loading used in this work is equivalent to a loading of 2 Mo atom/nm^2 for the alumina used, but the A_{BET} of the ASA(15) is almost twice that of alumina; thus, for the ASA(15) the equivalence is 1 Mo atom/nm^2. Considering that the ASA supports would be composed of a mixed oxide phase diluted in a separated alumina phase, the ASA(15) would have the highest concentration of the segregated alumina phase, and consequently, its PZC will be close to the one of alumina. Thus, the unexpected majority presence of distorted tetrahedral Mo species on ASA(15) would be explained by its high A_{BET}. The other ASA supports also have high surface areas, but with increasing the Si/(Si + Al) ratio, the PZC decrease [13], explaining the increase in the polymeric Mo species population at expense of the monomeric ones.

UV–vis DRS of the oxide catalysts in the 200–800 nm range were plotted in Fig. 5. Mo bands appear in the UV region (Fig. 5a) whereas Co bands appear in the visible one (Fig. 5b) [30,32,33]. Mo bands below 250 nm are commonly attributed to tetrahedral molybdate and the shoulder at 270-320 to octahedral molybdate [30,32,33]. It is observed that as showed above in the Raman results, the CMA catalyst is composed by a mixture of tetrahedral and octahedral molybdates. By this technique, it is observed a tendency of the distribution of Mo species with increasing the Si/(Si + Al) ratio similar to the one observed by Raman. CMS15 and CMS25 catalysts present a majority of tetrahedral species with only a little shoulder at the position where Mo-octahedral bands usually appear. DRS of these two catalysts are very similar in the UV region, consistent with what was observed in Raman's results. With the further increments in the Si/(Si + Al) ratio, it is observed that the shoulder corresponding to Mo octahedral increases, and thus the ratio octahedral Mo/tetrahedral Mo also increases, which is also consistent with Raman's results.

Regarding Co oxide species, in the spectra of the CMA catalysts a triplet at ca. 540, 580 and 630 nm is clearly observed, which according to literature it is related to tetrahedral Co species [30,33]. These tetrahedral Co species correspond to the existence of $CoAl_2O_4$ [30,33]. It is observed that with increasing the Si/(Si + Al) ratio, the triplet is less resolute indicating the decrease of the tetrahedral Co species. Again, it is remarkable that the CMS15 and the CMS25 catalysts present very similar DRS in the visible region. It is also observed that the band at 630 nm disappears progressively, and the band at 540 nm is shifted to lower wavelengths which according to Herrera and Resasco [28] indicates the presence of Co-octahedral species as those found in $CoMoO_4$ species. This is specially observed for the CMS33 and CMS50 catalysts. On the other hand, little bands at 450 and 750 nm are observed for the CMS50 and CMS75 catalysts, which according to literature indicate the presence of Co_3O_4 [28,30,33]. Thus, the Si/(Si + Al) affects the distribution of not only the Mo oxide species but the Co oxide ones.

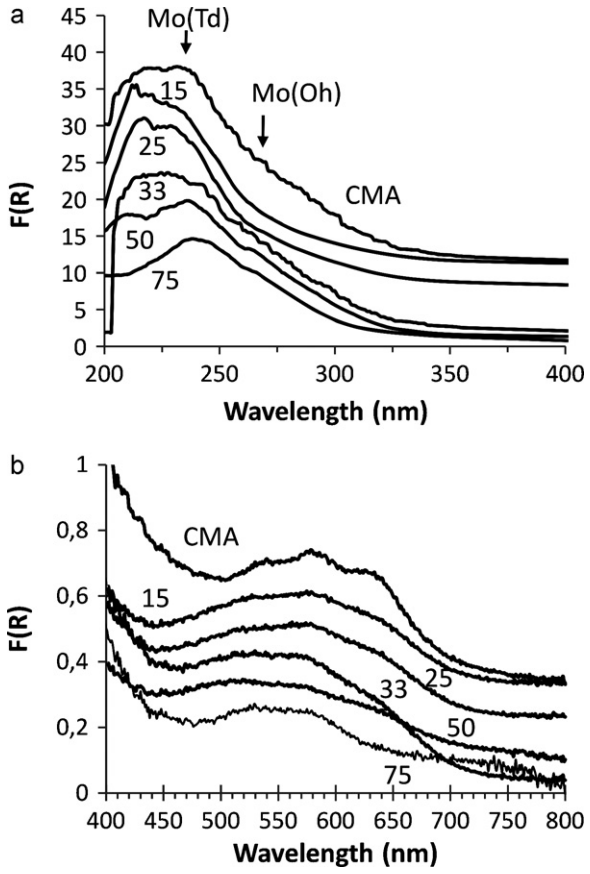

Fig. 5. UV–vis DRS of the ASAxx supported CoMo catalysts compared with the one supported on alumina (CMA). xx: % Si/(Si + Al).

Since octahedral Mo species are associated with polymeric species and tetrahedral ones are associated with monomeric species, it is possible to have an idea of the molybdenum dispersion from the distribution of these species. Thus, from the already described UV–vis DRS and Raman's results, it could be inferred that when increasing the Si content in the support, the dispersion of the Mo phase decreases. This fact is expected since Mo supported on pure silica has poor dispersion [14,28,32,33].

3.2. Influence of the Si/(Si + Al) ratio on the catalytic performance in the HDT of FCC naphtha

A lot of organic substances were found in the condensable products at the reactor outlet. A complete identification of all reaction products was done. We have already proposed reaction schemes for 2-MT and ramified olefins (TM1P and TM2P) [34] based on the product identification along with the comparison with other reaction schemes proposed in the literature [1,5–8,11,12,35]. These schemes are described below.

It has to be taken into account that both kinds of ramified olefins (TM1P and TM2P) are present in the feedstock; thus, there was equilibrium between them related to the double-bond isomerization either from internal to terminal positions or from terminal to internal positions [8,12]. The HYDO product was isooctane (iC8), the cracking ones were isobutene and isobutane (iC4s), and the skeletal isomerization ones (iC8-ske) were other trimethylpentenes (TMP) different from 2,4,4-TMPs and dimethylhexenes in a lower proportion [8,12]. The yield of oligomerization products was close to 1%; thus, they were not taken into account in the product distribution. On the other hand, thiols were not observed, at least in quantifiable concentrations. Thiol productions reported in other papers [5,8,12] were always low, and according to Hatanaka et al. [5] who studied the influence of various olefins in thiols production, 2,4,4-TMPs registered the lowest production in comparison with other olefins such as 1-octene, 1-hexene and cyclohexene. They also found that thiols derived from 2,4,4-TMPs were only detected after H_2S extra-addition in the feed [5].

Regarding 2-MT, a typical HDS scheme is observed with 2-methyltetrahydrothiophene (2-MTHT) as the main intermediate product from the hydrogenation pathway, and C5 hydrocarbons (C5s) as the final HDS products [1,5,8,35]. On the other hand, alkylmethylthiophenes (AMT) are also observed as product of the alkylation of 2-MT with olefins present in the reaction environment [6–8]. The most abundant was isobutylmethylthiophene, product of the reaction of isobutene with 2-MT. However, pentylmethylthiophenes and isooctylmethylthiophene were also detected in minor amounts.

The yield of the products listed above (continuous lines) and the reactant apparent kinetic constants (dotted lines) were plotted as a function of the Si/(Si + Al) ratio in Fig. 6. In Fig. 6a, the 2-MT apparent kinetic constant and its product distribution are shown; the same is shown for the TM1P and TM2P in Fig. 6b. The zero value in the *X*-axis represents the CMA catalysts. The product distribution was found to strongly depend on the Si/(Si + Al) ratio of the support used to prepare the catalysts. The 2-MT apparent kinetic constant over the ASA-supported catalysts was higher or at least at the same level than the one observed for the conventional catalysts. In the case of CMA, the main 2-MT products were C5s resulting from the HDS reaction, and as secondary product, a small yield to 2-MTHT was also observed. In general, an increase in the alkylation yield together with a simultaneous decrease in the HDS one was observed when increasing the Si/(Si + Al) ratio. However, it is noticeable that this augmentation of the alkylation yield at expense of the HDS one was not gradual; an abrupt change in the products distribution is observed in the region between 15 and 25% Si/(Si + Al). Thus, it can be said that this is a kind of transition

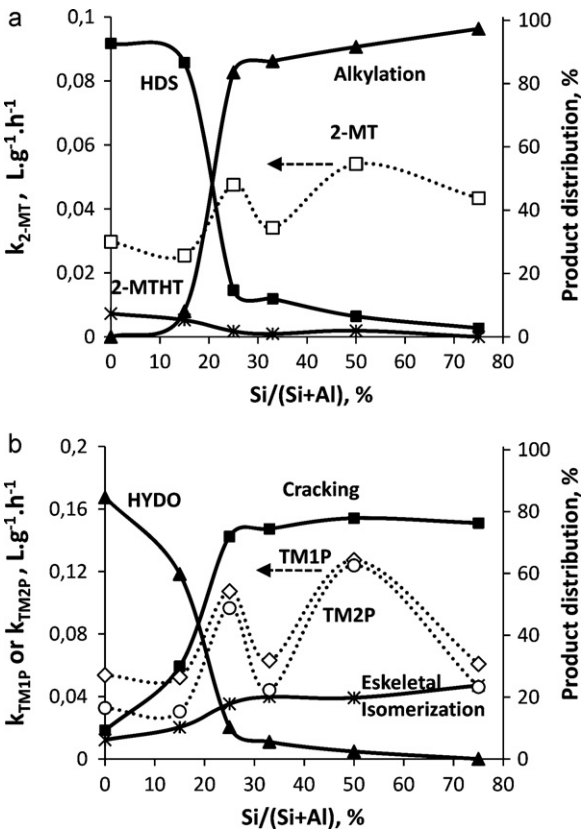

Fig. 6. Influence of the Si/(Si + Al) ratio on the reactives apparent kinetic constant (doted lines) and product yields (continuous lines) of the ASA-supported CoMo catalysts.

zone between catalysts that are more selective to HDS and those that are more selective to alkylation. Fig. 6b shows that the tendency of TM1P and TM2P apparent kinetic constants and the olefin product distribution are similar to those obtained with 2-MT. It is observed that as the Si/(Si + Al) ratio increases, acid-type reactions – skeletal isomerization, and cracking of olefins – become prevalent at the expense of the HYDO activity, and again an abrupt change is observed between the catalysts with 15 and 25% Si/(Si + Al). For the Si-rich catalysts, equilibrium between cracking and skeletal isomerization of olefin reactions was reached; however, comparing Si-rich catalysts with the Al-rich ones, the increase in the cracking activity was higher than the one of the skeletal isomerization activity.

Taken into account the great complexity of the reaction system when ASA supported catalysts are used; the selectivity HDS/HYDO, usually presented in literature [8], is not adequate to completely analyze the catalytic performance. In this work, we decided to apply a definition of the selectivity to HDS taking into account acid-type reactions. Therefore, the selectivity to HDS (S^{HDS}) was defined as the ratio between the 2-MT HDS activity and the addition of olefin cracking and HYDO activities (Eq. (5)). Cracking reaction was also included in the denominator because the products of this reaction are gaseous, causing a decrease in gasoline production, which must also be avoided [1,4,5]. On the contrary, the products from the skeletal isomerization are not included because they have a similar octane number to the one of 2,4,4-TMPs [36]; thus, their production is favorable because it does not affect the octane number and it is in competition with HYDO and cracking.

$$S^{HDS} = \frac{\text{2-MT HDS reactivity}}{\text{HYDO reactivity} + \text{Cracking reactivity}} \quad (5)$$

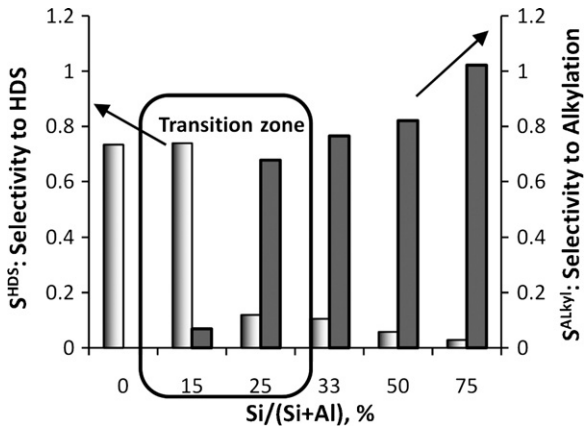

Fig. 7. Influence of the Si/Si + Al ratio on the ASA supported CoMo catalysts selectivities to HDS and alkylation.

The case of 2-MT is a little bit more complicated; the production of AMT is not good from the viewpoint of a classical HDS process because these kinds of products are also sulfur-containing compounds, and they are even more difficult to desulfurize. However, the boiling point of AMT is higher enough to allow its separation by distillation. In fact, a commercial alternative desulfurization based in this type of reactions was developed by the British Petroleum and named olefinic alkylation of thiophenic sulfur (OATS) [6,7]. Therefore, the production of AMT is a reaction, which can be potentially part of a desulfurization process. Having into account that alkylation competes with HDS in the transformation of 2-MT, a selectivity to alkylation (S^{Alkyl}) was defined in the same terms of the S^{HDS} (Eq. (6)) to quantify somehow the inclination of the catalysts to produce alkylation products:

$$S^{Alkyl} = \frac{\text{Alkylation reactivity}}{\text{HYDO reactivity} + \text{Cracking reactivity}} \quad (6)$$

The above-defined selectivities were plotted as a function of the Si/(Si + Al) ratio in Fig. 7. As it can be predicted from the activity results, the general trend is a diminution of S^{HDS} and an increase of S^{Alkyl} when increasing the Si/(Si + Al) ratio. The CMA exhibited a high S^{HDS} and a zero value of S^{Alkyl}; meanwhile, the CMS15 catalyst exhibited a value of S^{HDS} similar to the one of CMA accompanied by a low one of S^{Alkyl}, and again an abrupt change in the selectivity with a decrease in the S^{HDS} and an increase in S^{Alkyl} was observed for the CMS25. Beyond that point, a continuous but gradual decrease is observed in the S^{HDS}, at the same time that a continuous and gradual increase of the S^{Alkyl} was observed with the increase in the Si/(Si + Al) ratio.

Therefore, according to the catalytic behavior observed in Figs. 6 and 7, the catalysts could be divided into two groups in the studied Si/(Si + Al) range. The first group of catalysts is composed by the CMA and CMS15 catalysts, and the second group is composed by those supported on ASA with a Si/(Si + Al) ratio $\geq$0.25. It is quite interesting that inside these groups, the changes in product distribution and selectivities are gradual, but despite the small difference in the Si/(Si + Al) ratio between the catalysts in the boundary of both groups, CMS15 and CMS25, the changes in product distribution and selectivities are huge. Thus, this constitutes a transition zone between the catalysts that preferably promote HDS and HYDO reactions and those that promote acid-type ones. This transition zone could be explained considering that ASA-supported CoMo catalysts combine HDS, HYDO, and the acid-type functions in the same catalyst; thus, reacting molecules (2-MT and olefins) have the possibility to adsorb and transform in many different sites, and the preference of one or the other reaction will be related to the relative population and the activity of the different sites.

In the present work, the catalyst performances are compared at the same reaction conditions, and thus, it could not be compared at equivalent conversion. It is known that in some cases differences in selectivity and product distributions could arise simply by differences in conversions; however, this occurs mostly in the case of consecutive reactions, and in the present work the reactions considered are parallel to each other [37]. On the other hand, it could be observed for instance that CMS33 and CMS75 have comparable values of the reactant apparent kinetic constants to the ones of CMS15 and CMA, but there are considerable differences in the product distributions. Thus, it could be considered that the changes in product distribution observed when the Si/(Si + Al) was increased are real and they are not an illusion caused by the differences in reactant conversion.

According to discussed in Section 3.1, the distribution of Mo and Co species in the oxide state and the acid properties of the catalysts are strongly modified when the Si/(Si + Al) ratio was increased. However, regarding the distribution of Mo and Co species in the oxide state, its changes as a function of the Si/(Si + Al) ratio do not seem to be in agreement with those of the catalytic performance. This fact is especially observed in the transition zone. Although an abrupt change in the product distribution is observed between the CMS15 and the CMS25 catalysts, their distribution of Co and Mo species in the oxide state are quite similar as indicated by UV–vis and Raman spectra. Thus, the selectivity changes observed in the transition zone do not seem to be provoked by variations in the Co–Mo phase. However, the product distribution tendencies observed inside the two groups of catalysts before and after the transition zone could be explained, at least in part, by the differences in the distribution of Co and Mo species in the oxide state.

For instance, the catalytic performances of CMA and CMS15 catalysts were quite similar, with the highest S^{HDS} and HDS activity, but the distributions of the Mo species in the oxide state were quite different. The CMA catalysts exhibit a mixture of octahedral polymeric and tetrahedral monomeric Mo species with prevalence of the octahedral ones, whereas the CMS15 exhibits a majority of distorted tetrahedral monomeric species. It is considered that the undistorted tetrahedral monomeric Mo, although easier to reduce than the undistorted ones, are harder to reduce/sulfidate than the octahedral polymeric ones, and consequently, less active [33,35]. However, it should also be considered that the presence of the undistorted tetrahedral Mo species could improve the Mo dispersion [28,35], thus, compensating somehow that they are harder to reduce/sulfidate. Additionally, it was observed that the CMS15 catalyst has less quantity of $CoAl_2O_4$ than the CMA, and it is known that this compound is catalytically inactive [30,33]. These facts could explain why the HDS activity of the CMS15 is quite similar to the one of CMA despite of their different distributions of Mo and Co oxide species.

On the other hand, considering the group of catalysts after the transition zone (% Si/(Si + Al) > 25), a gradual increment in the acid type reaction yields at expense of an also gradual reduction of the HDS and HYDO yield is observed. This behavior could be explained up to certain extent by the decrease in the Mo dispersion evidenced in the UV–vis DRS and Raman spectra with the increment in Mo octahedral polymeric species when the Si/(Si + Al) ratio was increased. Additionally, the increasing presence of Co_3O_4 bands in the UV–vis DRS could also contribute to the reduction of the HDS and HYDO capacities of this group of catalysts when increasing the Si content [27,28,33]. Thus, it could be said that although the differences in the Co and Mo distribution could have some incidence in the catalytic performance of the catalysts, in this case they are not their main cause.

Conversely, changes in the acid properties with the Si/(Si + Al) ratio seem to be more related to the catalytic performance. Acid-type reactions such as isomerization and cracking of olefins, as well

as alkylation of 2-MT with olefins are accepted to proceed via carbenium ion intermediates, which normally need the presence of a Brönsted acid site to take place [11,20,38,39]. Thus, when both acid-type (especially Brönsted) and coordinative unsaturated sites (CUS) of Mo promoted by Co are present on the catalysts surface, the acid-type reactions are more energetically favorable than HDS or even HYDO [1,39]. The comparatively very low energy needed to perform the acid-type reactions [39] in comparison with HDS and HYDO causes that when the acid-sites density and strength increase, reactant molecules adsorb preferentially in this kind of sites, thus, competing with the adsorption in CUS sites. As a consequence, the HDS and HYDO reactions are inhibited, as described above. Also it is important to take into account that according to the literature, weaker Brönsted acid sites are able to perform isomerization reactions, whereas stronger Brönsted acid sites are needed for cracking and alkylation [39]. This fact could justify the existence of a point beyond which, the increment of Brönsted acid site density and strength gives origin to a preference of reactants to react via cracking and alkylation instead of HDS and HYDO. In our case, this point would be located somewhere in the aforementioned transition zone. In Fig. 2, it can be observed that at 373 K the Brönsted/Lewis ratio is quite similar for the CMS15 and the CMS25 catalysts, but at 473 and 573 K, it is higher for CMS25 than for CMS15, especially at 573 K where the Brönsted/Lewis ratio is very low for the CMS15 and the other ASA-supported ones have very similar values. Thus, the aforementioned transition zone could be due to the existence of strong Brönsted sites in the catalysts supported on ASA with Si/(Si + Al) ratio $\geq$0.25, which does not exist at all or in enough quantity in catalysts with Si/(Si + Al) ratio $\leq$0.15.

So far, we have discussed the existence and the possible causes of a transition zone between HDS-type catalyst and acid-type ones. As we already said above, all acid-type reactions are not detrimental to the objective of improving the selectivity to HDS; however, what we have not mentioned is that some of these reactions (double-bond and skeletal isomerization reactions) could even help to improve it. It has been shown in the literature that the isomerization of the double bond can play an important role in avoiding the HYD of the ramified olefins [8,12,34]. Terminal olefins are much easier to hydrogenate than internal ones [1,3,4,12]. This is explained by the steric effect caused by the substitution of hydrogen atoms linked to carbon atoms making part of the double bond [40]. Therefore, it will be desirable to avoid the double-bond isomerization from internal to terminal olefins or even displace the equilibrium of the reaction to produce internal olefins from terminal ones. Skeletal isomerization was also a beneficial reaction, not only because its products have similar octane number than 2,4,4-TMPs, but also due to its competition with HYDO and cracking reactions.

In Fig. 6, it is observed that both skeletal isomerization and cracking activities increase when increasing the Si content, but cracking increment is more accentuated. This can be explained because isomerization reactions are easier to perform by the weak acid sites and the increase in Brönsted/Lewis ratio, acid site density and strength promotes the activity in cracking reactions [39]. However, for the three catalysts with higher Si contents, equilibrium between both reactions was found. The equilibrium between both reactions is due to the skeletal isomerization reaction, which mainly produces other TMP (2,3,4-TMP and 3,4,4-TMP) different from 2,4,4-TMP and a few dimethylhexenes, and, thus, inhibiting in some way the cracking. The cracking of 2,4,4-TMP proceeds via a type A β-scission, which involves the formation of a tertiary carbenium ion to produce also another carbenium ion (isobutene). This is the most energetically favorable type of β-scission [20,38] and is the most probable mechanism to explain our results, because our principal cracking products were only isobutene and isobutane. On the contrary, the cracking of the other TMP and dimethylhexenes proceeds via type B1 or B2 β-scission, which starts with a secondary ion to finish with a tertiary one, and starts with a tertiary ion to finish with secondary one respectively [38]. Both type B β-scissions are much less energetically favored than type A β-scissions [38]. Thus, the skeletal isomerization plays a double role: on the one hand, controlling the HYDO, and on the other hand, controlling the cracking.

As a general remark, it can be said that when ASA is used as support for naphtha HDT catalysts, it is possible to manipulate the catalytic functions HDS, HYD, and acid type by changing the support Si/(Si + Al) ratio and, therefore, the acid properties. However, the manipulation of only the Si/(Si + Al) ratio was not enough to control finely the acidity of these materials in order to promote selectively the double-bond and skeletal isomerization, avoiding the undesirable olefin cracking; thus, inhibiting the HYDO, but not the HDS.

4. Conclusions

With increasing the Si/(Si + Al) ratio, the activity of the acid-type reactions was enhanced at expense of the activity of HDS and HYDO. The changes in selectivity and product distribution were not gradual. A kind of transition zone was observed between 15 and 25% Si/(Si + Al), where changes in selectivity and product distribution were surprisingly huge. This fact matches with an increment in the Brönsted acid sites density and strength. After its value reaches certain a point in the transition zone, the competition of the Brönsted sites with CUS for the reactants adsorption gives origin to a preference to react via cracking and alkylation instead of HDS and HYDO.

It was established that in addition to the control effect that double-bond isomerization from external to internal olefins exerts over HYDO, skeletal isomerization could also contribute in the control of this reaction, as well as cracking. Consequently, promotion of skeletal isomerization could aid to the preservation of octane number during FCC naphtha HDT.

It was demonstrated that by modifying the support composition, it is possible to manipulate the three basic catalytic functions of the catalysts: HDS, HYDO and acidity.

Acknowledgements

This work was possible due to the financial support of the VIE-UIS in the frame of the project: “Estudio de la influencia de la naturaleza de la carga y de la temperatura en la HDS de la nafta de craqueo” code 5434. D.J. Pérez-Martínez thanks COLCIENCIAS and UIS for the Ph.D. fellowship. Authors especially thank to L.G. Guzman for the detailed revision of the English language in this article.

References

[1] S. Brunet, D. Mey, G. Pérot, C. Bouchy, F. Diehl, Appl. Catal. A 278 (2005) 143–172.
[2] C. Song, Catal. Today 86 (2003) 211–263.
[3] T.G. Kaufmann, A. Kaldor, G.F. Stuntz, M.C. Kerby, L.L. Ansell, Catal. Today 62 (2000) 77–90.
[4] S. Hatanaka, M. Yamada, O. Sadakane, Ind. Eng. Chem. Res. 36 (1997) 1519–1523.
[5] S. Hatanaka, M. Yamada, O. Sadakane, Ind. Eng. Chem. Res. 36 (1997) 5110–5117.
[6] V. Belliere, C. Geantet, M. Vrinat, Y. Ben-Taarit, Y. Yoshimura, Energy Fuels 18 (2004) 1806–1813.
[7] M. Arias, D. Laurenti, V. Bellière, C. Geantet, M. Vrinat, Y. Yoshimura, Appl. Catal. A 348 (2008) 142–147.
[8] D. Mey, S. Brunet, C. Canaff, F. Maugé, C. Bouchy, F. Diehl, J. Catal. 227 (2004) 436–447.
[9] S. Hatanaka, T. Miyama, H. Seki, S. Hikita, EP 0736589 A1 (1996).
[10] C. Flego, V. Arrigoni, M. Ferrari, R. Riva, L. Zanibelli, Catal. Today 65 (2001) 265–270.
[11] G. Muralidhar, F.E. Massoth, J. Shabtai, J. Catal. 85 (1984) 44–52.

[12] M. Toba, Y. Miki, T. Matsui, M. Harada, Y. Yoshimura, Appl. Catal. B 70 (2007) 542–547.
[13] V. La Parola, G. Deganello, A.M. Venecia, Appl. Catal. A 260 (2004) 237–247.
[14] V. La Parola, G. Deganello, S. Scirè, A.M. Venecia, J. Solid State Chem. 174 (2003) 482–488.
[15] J.B. Miller, I.E. Ko, Catal. Today 35 (1997) 269–292.
[16] V.L. Barrio, P.L. Arias, J.F. Cambra, M.B. Güemez, B. Pawelec, J.L.G. Fierro, Fuel 82 (2003) 501–509.
[17] P. Berteau, B. Delmon, Catal. Today 5 (1989) 121–137.
[18] J.-P. Damon, B. Delmon, J.M. Bonnier, J. Chem. Soc., Faraday Trans. 1 73 (1977) 372–380.
[19] P.O. Scokart, F.D. Declerck, R.E. Sempels, P.G. Rouxhet, J. Chem. Soc., Faraday Trans. 1 73 (1977) 359–371.
[20] G. Busca, Chem. Rev. 107 (2007) 5366–5410.
[21] C. Defossé, P. Canesson, P.G. Rouxhet, B. Delmon, J. Catal. 51 (1978) 269–277.
[22] R.E. Sempels, P.G. Rouxhet, J. Colloid Interface Sci. 55 (1975) 263–273.
[23] H. Knözinger, P. Ratnasamy, Catal. Rev. Sci. Eng. 17 (1978) 31–70.
[24] T.J. Bandoz, Ch. Lin, J.A. Ritter, J. Colloid Interface Sci. 198 (1998) 347–353.
[25] B. Xu, C. Sievers, J.A. Lercher, J.A. Rob van Veen, P. Giltay, R. Prins, J.A. van Bokhoven, J. Phys. Chem. C 111 (2007) 12075–12079.
[26] C. Sârbu, B. Delmon, Appl. Catal. A 185 (1999) 85–97.
[27] V. La Parola, G. Deganello, C.R. Tewell, A.M. Venezia, Appl. Catal. A 235 (2002) 171–180.
[28] J.E. Herrera, D.E. Resasco, J. Catal. 221 (2004) 354–364.
[29] G. Mestl, T.K.K. Srinivasan, Catal. Rev. Sci. Eng. 40 (1998) 451–570.
[30] B. Pawelec, T. Halachev, A. Olivas, T.A. Zepeda, Appl. Catal. A 348 (2008) 30–41.
[31] C.C. Williams, J.G. Ekerdt, J.-M. Jehng, F.D. Hardcastle, I.E. Wachs, J. Phys. Chem. 95 (1991) 8791–8797.
[32] H. Jeziorowski, H. Knözinger, P. Grange, P. Gajardo, J. Phys. Chem. 84 (1980) 1825–1829.
[33] J. Vakros, A. Lycourghiotis, G.A. Voyiatzis, A. Siokoub, C. Kordulis, Appl. Catal. B 96 (2010) 496–507.
[34] D.J. Pérez-Martínez, S.A. Giraldo, A. Centeno, Appl. Catal. A 390 (2010) 59–70.
[35] H. Topsoe, B.S. Clausen, F.E. Massoth, in: J.R. Anderson, M. Boudart (Eds.), Hydrotreating Catalysis, Science and Technology, Springer-Verlag, Berlin, 1996.
[36] W. Gruse, D. Stevens, The Chemical Technology of Petroleum, 2nd ed., McGraw Hill, New York, 1942.
[37] G.F. Froment, K.B. Bischoff, Chemical Reactor Analysis and Design, 2nd ed., Wiley, 1990.
[38] J.S. Buchanan, J.G. Santiesteban, W.O. Haag, J. Catal. 158 (1996) 279–287.
[39] A. Corma, Chem. Rev. 95 (1995) 559–614.
[40] F.A. Carey, Química Orgánica, 3ª ed., McGraw Hill, Madrid, 1999.